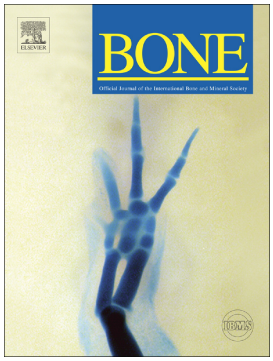

Statistical analysis of the inter-individual variations of the bone shape, volume fraction and fabric and their correlations in the proximal femur

Elham Taghizadeh, Vimal Chandran, Mauricio Reyes, Philippe Zysset, Philippe Büchler

PII: S8756-3282(17)30238-7
DOI: doi: 10.1016/j.bone.2017.07.012
Reference: BON 11369

To appear in: *Bone*

Received date: 20 February 2017
Revised date: 22 June 2017
Accepted date: 11 July 2017

Please cite this article as: Elham Taghizadeh, Vimal Chandran, Mauricio Reyes, Philippe Zysset, Philippe Büchler , Statistical analysis of the inter-individual variations of the bone shape, volume fraction and fabric and their correlations in the proximal femur, *Bone* (2016), doi: 10.1016/j.bone.2017.07.012

Statistical Analysis of the Inter-Individual Variations of the Bone Shape, Volume Fraction and Fabric and Their Correlations in the Proximal Femur

Elham Taghizadeh, Vimal Chandran, Mauricio Reyes, Philippe Zysset and Philippe Büchler

Institute for Surgical Technology and Biomechanics (ISTB), University of Bern

Address for correspondence:
Philippe Büchler
Institute for Surgical Technology & Biomechanics
University of Bern
Stauffacherstrasse 78
3014 Bern, Switzerland
Email: philippe.buechler@istb.unibe.ch

Abstract

Including structural information of trabecular bone improves the prediction of bone strength and fracture risk. However, this information is available in clinical CT scans, only for peripheral bones. We hypothesized that a correlation exists between the shape of the bone, its volume fraction (BV/TV) and fabric, which could be characterized using statistical modeling. High-resolution peripheral computed tomography (HR-pQCT) images of 73 proximal femurs were used to build a combined statistical model of shape, BV/TV and fabric. The model was based on correspondence established by image registration and by morphing of a finite element mesh describing the spatial distribution of the bone properties. Results showed no correlation between the distribution of bone shape, BV/TV and fabric. Only the first mode of variation associated with density and orientation showed a strong relationship ($R^2 > 0.8$). In addition, the model showed that the anisotropic information of the proximal femur does not vary significantly in a population of healthy, osteoporotic and osteopenic samples. In our dataset, the average anisotropy of the population was able to provide a close approximation of the patient-specific anisotropy. These results were confirmed by homogenized finite element (hFE) analyses, which showed that the biomechanical behavior of the proximal femur was not significantly different when the average anisotropic information of the population was used instead of patient-specific fabric extracted from HR-pQCT. Based on these findings, it can be assumed that the fabric information of the proximal femur follows a similar structure in an elderly population of healthy, osteopenic and osteoporotic proximal femurs.

Keywords: Statistical model, Bone properties, Proximal femur, Average fabric tensor, HR-pQCT

1 Introduction

The introduction of micro-computed tomography enabled a detailed description of bone architecture. Many measures have been extracted from these images to quantify bone micro-architecture such as volume fraction, orientation, or trabecular thickness. Correlation of these morphometric measurements with bone mechanics showed that only two of these parameters – the bone volume fraction (BV/TV) and bone fabric – are responsible for 98% of the trabecular bone stiffness and yield strength [1,2]. More specifically, bone volume fraction showed a correlation of 80%-90% with bone stiffness and 79% correlation with yield strength, while bone fabric correlated up to 10 – 20% with bone stiffness and 23% correlation with yield strength. Therefore, these parameters are critical to build patient-specific models and assess individual fracture risks.

In the clinical situation, BV/TV can be estimated from Hounsfield Units (HU) reconstructed in CT scans. However, since it is not possible to obtain images of the bone micro-structure *in vivo*, several methods have been proposed to determine the most probable bone fabric from clinical resolution scans of the patient's bone. Some authors proposed to estimate the local anisotropy based on the outer shape of the bone [3,4] or based on the principal directions obtained from FE calculations, either from the principal strains of a homogenous model [5] or during an iterative approach progressively refining the anisotropic directions based on the principle stresses [6,7]. These approaches provide a global estimation of the anisotropic direction, however the accuracy of the eigenvalues associated with these directions is unknown. Other methods have been proposed based on pre-existing knowledge of the bone architecture. Some approaches rely on machine learning techniques to model the anisotropic information as a function of bone shape and/or distribution of the bone mineral density (BMD) [8–10]. Other studies rely on existing high-resolution scans to estimate the fabric tensor for clinical CT. Hazrati and colleagues employed a database of high-resolution scans and assigned to the patient's bone the anisotropy of the closest instance in a pre-existing database. A similar study has been conducted where a single template anisotropy was morphed into the shape of the patient's bone [11]. Interestingly, while a single template was used to estimate bone anisotropy, the prediction error was in the same range as for the studies that employed a dataset of high-resolution scans [11]. This result questions the variability of bone anisotropy

among individuals and indicates that the good predictions reported previously could be a consequence of a low inter-subject variability.

The variations in the structural parameters of bones were usually studied only for specific parts, e.g. femoral head or femoral neck [12–14] and were not compared to the corresponding bone morphology. Several studies aimed at providing a correlation between parameters describing the bone architecture with fracture risk [12,13] or with the age of the patients [14]. However, these parameters were estimated on a single or few regions of the proximal femur. To the best of our knowledge, only one study reported the local variations of the bone structural properties for the complete bone [15]. They found a large coefficient of variation for BV/TV and trabecular parameters, but the coefficient of variation was small for Structural Model Index (SMI) and degree of anisotropy (DA). The results of these studies appear contradicting; while some authors reported a change of the DA –for example associated with increased fracture risk [12,13]– other studies reported only local variation of the DA [14] or even insignificant variation of DA in a small population without fracture [15]. In addition, while all these models describe local variations of micro-architectural parameters, no study provides a full description of the spatial distribution of the BV/TV, bone fabric, and morphology and how these distributions vary between subjects.

The aim of this study is to better characterize the distribution of bone fabric in the proximal femur of a population and to determine the variability of the overall fabric organization between individuals. Therefore, instead of using predictive or regression models, we build a generative model using principal component analysis (PCA), that finds the variations of bone parameters in a given population. Such model helps to analyze the relation among different bone parameters. The initial underlying hypothesis was that these parameters are strongly correlated, and that a combined statistical model could reveal these correlations. In addition, based on the combined statistical model, the bone fabric information could be recovered at any spatial position relying only on the shape and BV/TV extracted from clinical-level CT scans.

2 Material and Methods

2.1 Dataset

A dataset of 73 proximal femurs [16] was used to build a statistical model of bone properties. The bones were obtained from 37 individual donors, 18 males and 19 females. The donors' ages were in the range of [46, 96] years with the average age of 76 ± 11 years. Based on available DEXA images, 39% of proximal femurs (28 samples) were classified as osteoporotic, 31% (23 samples) as osteopenic and 28% (20 samples) normal. Two samples had no DEXA scan available and were classified as unknown. From each bone, one HR-pQCT (Xtreme-CT, Scanco Medical, Switzerland) image with a spatial resolution of 0.082 × 0.082 × 0.082 mm was acquired. The images were obtained with an intensity of 900 µA and voltage of 60 kV. The Bone Mineral Density (BMD) values extracted from the HR-pQCT image were calibrated based on machine's settings. The BMD values then used to compute the BV/TV by applying reported calibration curve in the literature that maps BMD to the corresponding BV/TV [11,16]. The shafts of all samples were cropped such that they all have the same ratio between the shaft length and the neck length [9].

2.2 Establishing Correspondences

The first step in building a statistical model is to establish a spatial correspondence between the bones of the dataset. To build a statistical model relevant for bone biomechanical properties, correspondences must be established not only on the surface of the bone, but also for any points within the bone volume containing trabecular bone. For this reason, image registration was used to establish voxel-wise correspondences among the bones. This approach was chosen because image registration uses information on the outer shape as well as the bone intensity values inside the bone volume, which establishes a reliable correspondence also in the trabecular region [17]. Rigid, affine, and non-rigid image registrations were performed between the reference bone and each bone in the dataset. For the rigid registration, the bones were aligned with respect to the midpoint of the femoral neck [9]. It was followed by an affine registration to refine the global alignment. The final registration was performed using the B-spline method provided by the elastix software [18]. In this method multi-resolution grids are superimposed on the image.

At each resolution, the transformation is calculated as the sum of weighted B-spline basis functions on the control points of the grid.

The reference bone was selected through an iterative process. In the first step, one image in the database was selected arbitrarily as the template bone. All images were registered to this template bone and a new template bone was constructed based on the average of the registration displacement vectors. The process of computing a new average bone and registering all images to the image of this new mean shape was repeated until convergence, when the average bone does not change anymore. Finally, the closest bone in the dataset to the average was selected by using the Frobenius norm of the stretch tensor of the local deformation gradient. In this step, all bones in the dataset were registered to this reference bone.

An FE mesh of the reference bone with average edge length of 1 mm was created and morphed to all instances. This reference mesh was made of approximately 167000 linear tetrahedral elements. The morphing was performed using the displacement vector fields (DVF) obtained from the image registration step. As a result, all the bones had an FE mesh with the same number of elements, and with nodes positioned at corresponding anatomical locations.

2.3 Bone Volume Fraction and Fabric Information

The material properties of the bone were assigned to each element of the mesh using the method proposed by Pahr and Zysset [19]. In this method a mesh grid with a given distance between nodes is overlaid on the image. For each grid point, a spherical region of interest (ROI) was extracted and the BV/TV as well as the fabric tensor are calculated for this ROI. The material properties of each element were calculated by linear interpolation of the values computed for the neighboring grid nodes of each element.

In this study, the ROIs were selected as spheres having a diameter of 5.3 mm and the distance between grid points was equal to 2 mm. The BV/TV was extracted from the calibrated HR-pQCT scans and the Mean Intercept Length (MIL) method was used to estimate the fabric tensor of each ROI. In the final step, the FE mesh of all bones was aligned to the reference bone, using Procrustes analysis. The rotation found using Procrustes was then applied to the fabric tensors.

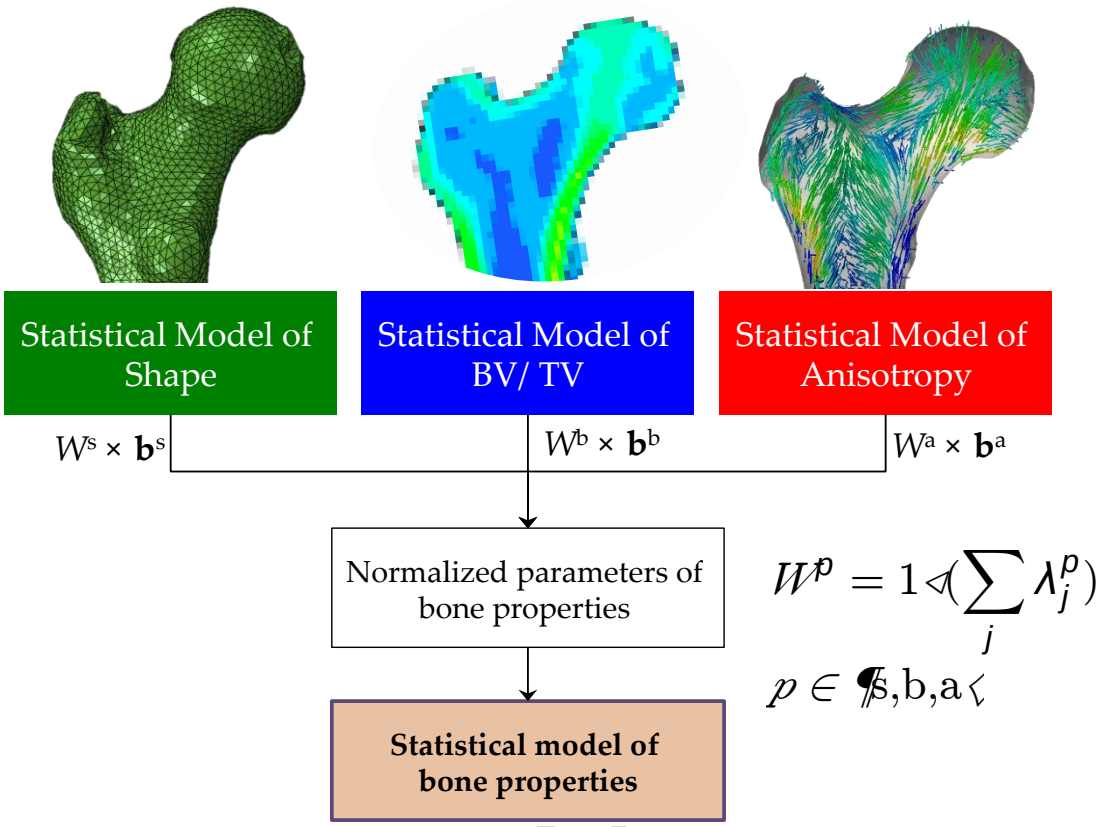

Figure 1. The pipeline for building statistical model of bone biomechanical properties. The statistical model of shape, BV/TV and anisotropy were built separately and were combined after appropriate normalization. The normalization weight of each model is calculated as the inverse of the sum of the eigenvalues (λ_j) of that model.

2.4 Statistical Models

The technique to build the statistical model was adapted from the procedure used to derive Statistical Appearance Models (SAM) [20]. Three distinct statistical models were computed: for 1) shape, 2) BV/TV, and 3) fabric tensor. The three models were combined in a second step. Each individual model was weighted to account for the different dimensionality of the respective reference models (Figure 1).

PCA was used for building statistical models. The PCA technique fits a hyper-ellipsoid to the input data, where the direction of largest diameters represent the direction of maximum variances in the data and the diameter length is the standard deviation in that direction [21]. To compute principal components, the data matrix **X** of size d × n (d is the dimension of each sample and n is the number of samples in the dataset) is centered ($\hat{\mathbf{X}}$) by subtracting the average of the data from each sample. The data covariance matrix is then formed as:

$$\mathbf{C} = \hat{\mathbf{X}}\hat{\mathbf{X}}^{\mathrm{T}}, \tag{1}$$

where superscript T stands for the transpose of the matrix. The spectral decomposition of the covariance matrix provides the eigenvectors and eigenvalues of the statistical model:

$$\mathbf{C} = \mathbf{Q}\mathbf{\Lambda}\mathbf{Q}^{-1}, \tag{2}$$

where Q contains the eigenvectors of matrix $\mathbf{C}$ and $\mathbf{\Lambda}$ is a diagonal matrix with eigenvalues on its main diagonal. If d > n (the data dimension is larger than the number of samples), the rank of matrix $\mathbf{C}$ is smaller or equal to n. In this case, to reduce the computational burden, the spectral decomposition is performed on the following matrix $\hat{\mathbf{C}}$:

$$\begin{aligned} \hat{\mathbf{C}} &= \hat{\mathbf{X}}^{\mathrm{T}}\hat{\mathbf{X}} \\ \hat{\mathbf{C}} &= \hat{\mathbf{Q}}\mathbf{\Lambda}\hat{\mathbf{Q}}^{-1} \end{aligned} \tag{3}$$

The eigenvalues ($\mathbf{\Lambda}$) computed in equations (**2**) and (**3**) are equal. Furthermore, the eigenvectors in equation (**2**) can be calculated as:

$$\mathbf{Q} = \hat{\mathbf{X}}\hat{\mathbf{Q}} \tag{4}$$

2.4.1 Statistical Model of Shape

The shape of each bone was represented by the coordinates of the centers of all the elements in the volumetric mesh. Each element was represented by a linear tetrahedron. The bone shape was represented as a matrix of size m × n, where n is the number of samples in the dataset and m = k × 3, with k is the number of elements in the mesh. PCA was applied to this matrix and the parameters of the model can be used to create a new sample shape as follows:

$$\mathbf{x}^s = \bar{\mathbf{x}}^s + \mathbf{Q}^s\mathbf{b}^s, \tag{5}$$

where $\mathbf{x}^s$ describes the shape of a bone and $\bar{\mathbf{x}}^s$ is the average shape of the bones in the dataset. The vector $\mathbf{b}^s$ contains the parameters of shape in the statistical model space and $\mathbf{Q}^s$ is the matrix of the corresponding eigenvectors. Each eigenvector is called a "mode" of variation. With this approach, any bone in the dataset can be described by a set of scalar values $\mathbf{b}^s$.

2.4.2 Statistical Model of Bone Volume Fraction

The same approach was used to build the model for the volume fraction. The BV/TV for all the bones in the dataset was described by a matrix of size k × n, where k is the number of elements in the mesh and n is the number of bones in the dataset. After PCA, BV/TV values for the new sample ($\mathbf{x}^b$) can be estimated with the following equation:

$$\mathbf{x}^b = \bar{\mathbf{x}}^b + \mathbf{Q}^b\mathbf{b}^b, \tag{6}$$

where $\bar{\mathbf{x}}^b$ is a vector with average BV/TV for each element in the dataset, $\mathbf{b}^b$ contains the parameters of the BV/TV model and $\mathbf{Q}^b$ is a matrix containing the corresponding eigenvectors.

2.4.3 Statistical Model of Bone Fabric Tensor

The anisotropic information is represented by orthogonal and positive-definite tensors. Applying arithmetic averaging and PCA calculations in the Euclidean space would result in invalid tensors that would not preserve these properties. One known problem is the tensor swelling effect [22]; With the arithmetic averaging, the determinant of the average tensor can become larger than the determinant of each individual tensor. In addition, covariance and PCA calculations are unable to preserve the positive definite property of the tensors (eigenvalues might become negative) [23]. To solve this problem, PCA was calculated in the log-Euclidean space as proposed by Arsigny et al. [22]. A logarithmic function was applied to each fabric tensor to map the tensors to the log-Euclidean space as follows:

$$\begin{aligned} \mathbf{M} &= \sum_{i=1}^{3} m_i \mathbf{m}_i \otimes \mathbf{m}_i \\ \mathbf{L} &= \log(\mathbf{M}), \end{aligned} \tag{7}$$

where m_i and $\mathbf{m}_i$ are eigenvalues and eigenvectors of the fabric tensor $\mathbf{M}$. The tensor $\mathbf{M}$ is normalized such that trace($\mathbf{M}$) = 3. The logarithm tensor was then vectorized as:

$$\mathrm{l} = \left[L_{11}, L_{22}, L_{33}, \sqrt{2}L_{12}, \sqrt{2}L_{13}, \sqrt{2}L_{23}\right], \tag{8}$$

where L_{ij} represents the element in the i^{th} row and j^{th} column of the log-tensor $\mathbf{L}$. After concatenating the log-Euclidean vectors for all elements of each bone into one vector

$\mathbf{x}^i$, the fabric information for all bones in the dataset can be described by the matrix $\mathbf{X}$, which size was $6k \times n$:

$$\begin{aligned} \mathbf{x}^i &= \left[\mathbf{l}_1^i, \mathbf{l}_2^i, \cdots, \mathbf{l}_k^i\right]^{\mathrm{T}} \\ \mathbf{X} &= \left[\mathbf{x}^1 \cdots \mathbf{x}^n\right], \end{aligned} \tag{9}$$

where k represents the number of elements and n is the number of bones in the dataset and superscript T represents the transpose of a vector. The anisotropy tensors for a new sample in the log-Euclidean space $\mathbf{x}^a$ were computed as:

$$\mathbf{x}^a = \bar{\mathbf{x}}^a + \mathbf{Q}^a \mathbf{b}^a, \tag{10}$$

where $\bar{\mathbf{x}}^a$ is the average of fabric tensors in the log-Euclidean space, $\mathbf{b}^a$ consists of the parameters of the fabric tensor anisotropy and $\mathbf{Q}^a$ is a matrix containing the eigenvectors of the statistical model of anisotropy. While $\mathbf{b}^a$ is a scalar value, the reconstructed anisotropy $\bar{\mathbf{x}}^a$ lies in the log-Euclidean space. Therefore, to reconstruct the anisotropy in the original Euclidean space, the procedures described by equations (**7**) and (**8**) should be inverted.

2.4.4 The Combined Model

To build a statistical model representing multimodal bone properties, an approach similar to the method used for statistical appearance modeling [20] was used. In our problem, the combined model was created by applying PCA to the combined scores of statistical models of the bone shape, BV/TV, and fabric. The combined scores were built as follows for the i^{th} bone in the dataset:

$$\mathbf{b}_i = \begin{pmatrix} w^s \mathbf{b}_i^s \\ w^b \mathbf{b}_i^b \\ w^a \mathbf{b}_i^a \end{pmatrix} = \mathbf{Q}\mathbf{c}, \tag{11}$$

where w^s, w^b, and w^a are weighting parameters for shape, BV/TV, and anisotropy. The matrix $\mathbf{Q}$ contains the eigenvectors of the combined model and $\mathbf{c}$ is a vector formed by the scores of the combined model. Weights were required to normalize the initial model, because each initial model describes a different physical quantity. The weights were calculated as

$$w^p = 1/\sum_j \lambda_j^p \tag{12}$$

where p indicates either shape, BV/TV, or fabric and λ_j^p are the eigenvalues of the corresponding bone properties. In the rest of paper, the 3-combined model phrase is used for the model including all three parameters of the bone.

2.5 Model Evaluation

2.5.1 Generalization Error

This metric can be calculated using the leave-one-out method. A model is built based on all the samples except one ($\mathbf{s}_i$), which is reconstructed by calculating its **b** parameters in the model space as:

$$\mathbf{b} = \mathbf{Q}^{-1}(\mathbf{s}_i - \bar{\mathbf{s}}), \tag{13}$$

where $\bar{\mathbf{s}}$ is the average of samples in the dataset without $\mathbf{s}_i$ and **Q** contains the eigenvectors of the model. Since the model does not encode all the possible variability, the reconstructed sample will differ from the original sample. This difference measures the performance of the statistical model. The process is repeated until the errors of reconstructing all samples in the dataset are computed. The generalization ability of the selected model is inversely proportional to the average reconstruction error.

Since in our dataset the bones were acquired from both legs of the donors, the reconstruction errors for each bone were calculated after excluding its pair from the training dataset. This precaution was taken to avoid a possible bias related to similarities between the left and right femurs of each individual.

For the fabric tensor, the error was measured with two metrics; the error on the reconstructed DA and the error on the principal fabric direction (PFD):

$$\begin{aligned} \mathrm{error}_{\mathrm{DA}} &= \frac{|\mathrm{DA} - \hat{\mathrm{DA}}|}{\hat{\mathrm{DA}}} \times 100 \\ \mathrm{error}_{\mathrm{PFD}} &= \arccos\left(\mathbf{m}_1 \cdot \hat{\mathbf{m}}_1\right), \end{aligned} \tag{14}$$

where, DA and $\mathbf{m}_1$ are the DA and principal direction extracted from HR-pQCT scan and $\hat{\mathrm{DA}}$ and $\hat{\mathbf{m}}_1$ are the same quantities reconstructed using the model. The symbol "." represents the inner product of two vectors.

2.5.2 Compactness

The compactness is calculated as the ratio between the first m eigenvalues divided by the sum of all the eigenvalues from the model:

$$C(m) = \frac{\sum_{i=1}^{m} \lambda_i}{\sum_{i=1}^{d} \lambda_i}, \tag{15}$$

Compactness describes the distribution of the data. A small compactness value indicates that the fitted shape to data using PCA is close to a hyper-sphere and a high compactness represent distributed data along a few vectors. In this context, high compactness means that a large variability can be represented by a low number of modes.

2.5.3 FE Simulations

We performed FE simulations to evaluate the mechanical effect of predicting the bone fabric based on a statistical model. The mesh used to quantify BV/TV and fabric was also used for the FE calculations. Therefore, the output of the combined model is directly compatible with the finite element method. To avoid possible element distortion after mesh morphing, linear tetrahedral were used for the calculations (by comparing the output of FE analyses with quadratic elements, the linear elements were found to be valid for the mesh density used in our FE analyses). The cortical bone was defined by all the elements having a BV/TV over 0.5 as well as the surface elements of the mesh. These elements were assigned cortical bone properties, the rest of the elements were considered to be the trabecular bone, which properties were based on the local BV/TV and fabric.

For this test, 10 left femurs (5 male and 5 female) were arbitrarily selected. Three of them were categorized as healthy, two as osteopenic and three as osteoporotic. Three different scenarios were tested: 1) with anisotropy extracted from HR-pQCT scans (original anisotropy), 2) using isotropic material properties and 3) employing the fabric tensor predicted using a statistical model. The bones were loaded in the stance position and an elastic-viscoplastic material model [24] was used to describe the tissue with previously published material constants provided in Table 1.

To validate the original model, the mechanical simulations were compared against experimental data. In the experiments, the head of the bones was displaced up to failure by a servo-hydraulic machine (Mini-Bionix, MTS system, USA) with a speed of 5 mm/min [25]. To show the importance of including bone fabric in hFE analysis, models with isotropic fabric were also compared to the mechanical tests. In this study, identical constitutive models and properties were used for both isotropic and orthotropic models. The isotropic models were defined by an isotropic fabric, having eigenvalues of one in each direction.

Table 1: Mechanical parameters for the elastic-visco plastic model used in the finite element simulations [16].

		E_0 [GPa]	ν_0	G_0 [GPa]	k	l	σ_0 [MPa]	χ_0	τ_0 [MPa]	η	M	Yield ratio
Trabecular	Tension	12	0.249	3.913	1.878	1.076	81.6	-0.3	68.9	1.2	4.0	0.66
	Compression						111.6	0.31				
Cortical	Tension	12	0.34	4.47	1.0	1.0	72.0	-0.37	62.6			
	Compression						108.0	0.49				

2.6 Statistical Analyses

The relations between different modes of shape, BV/TV, and fabric tensor were compared using the coefficient of determination (R^2). For the mechanical evaluation, the predicted ultimate force and displacement were compared between the different hFE models as well as with the experimental results. Linear regression and paired t-test were used to compare these calculations as well as an ANCOVA test to compare the slope of the different regressions. For all statistical analyses, differences with *p* values smaller than 0.05 were considered to be statistically significant.

3 Results

3.1 Model Evaluation

Four statistical models have been constructed based on the HR-pQCT datasets: three independent models for shape, BV/TV, and fabric as well as the 3-combined model. A qualitative comparison of the first modes of each individual model with the corresponding modes of the combined model indicated minor differences between both representations of the data, especially in the first mode of variation (Figure 2). As expected the overall influence on the bone shape, BV/TV, and DA decreased by

the increasing mode number. The samples created along each mode do not show a large difference between 3-combined model and the individual models. To better represent the underlying variation, the differences on the reconstructed bone parameters at ±2 times standard deviation ($\sqrt{\boldsymbol{\lambda_i^p}}$) were calculated. The difference for parameter p (shape, BV/TV or anisotropy) in the mode of i can be expressed as $\mathbf{D}_i^p = (\bar{\mathbf{x}}^p + 2\sqrt{\lambda_i^p}\mathbf{Q}_i^p) - (\bar{\mathbf{x}}^p - 2\sqrt{\lambda_i^p}\mathbf{Q}_i^p) = 4\sqrt{\lambda_i^p}\mathbf{Q}_i^p$). The first mode was very similar between the 3-combined and the individual model, but differences were visible in the second mode. However, the difference between the 3-combined and the individual models remained small compared to the average bone and did not significantly affect the overall distribution of bone shape, BV/TV, DA, or the fabric orientation. The difference in the principal orientation of the bone was represented as the angle between the principal directions of the reconstructed fabric tensor at $\pm 2\sqrt{\boldsymbol{\lambda_i^p}}$ distance from the mean tensor (Figure 2). While the average variation in the principal tensor direction in the first mode of the 3-combined model and individual tensor model was only 19 ± 22 degrees, for some elements the variation reached up to 90 degrees. These elements were mostly located on the regions where the tensor is almost isotropic. Elements on the intertrochanteric line also showed a large variation of the orientation for different modes of the model. This region is located at the border between two different trabecular bone textures. Consequently, small variations in the location of elements can result in a difference of 90 degrees in the principal direction of the fabric tensor.

The relationship between the different morphometric parameters was evaluated using the correlations between the parameters of the different statistical models; shape, BV/TV and fabric (Figure 3). For each bone, the "b-parameters" and all possible correlations between the parameters were quantified. No correlation was found except one between the first modes of BV/TV and fabric tensor models (R2 = 0.8). This strong correlation indicates that the change in overall bone density in the population (described by the first mode of BV/TV) is associated with a change in the bone fabric distribution. None of the other correlations was above $R^2 = 0.5$.

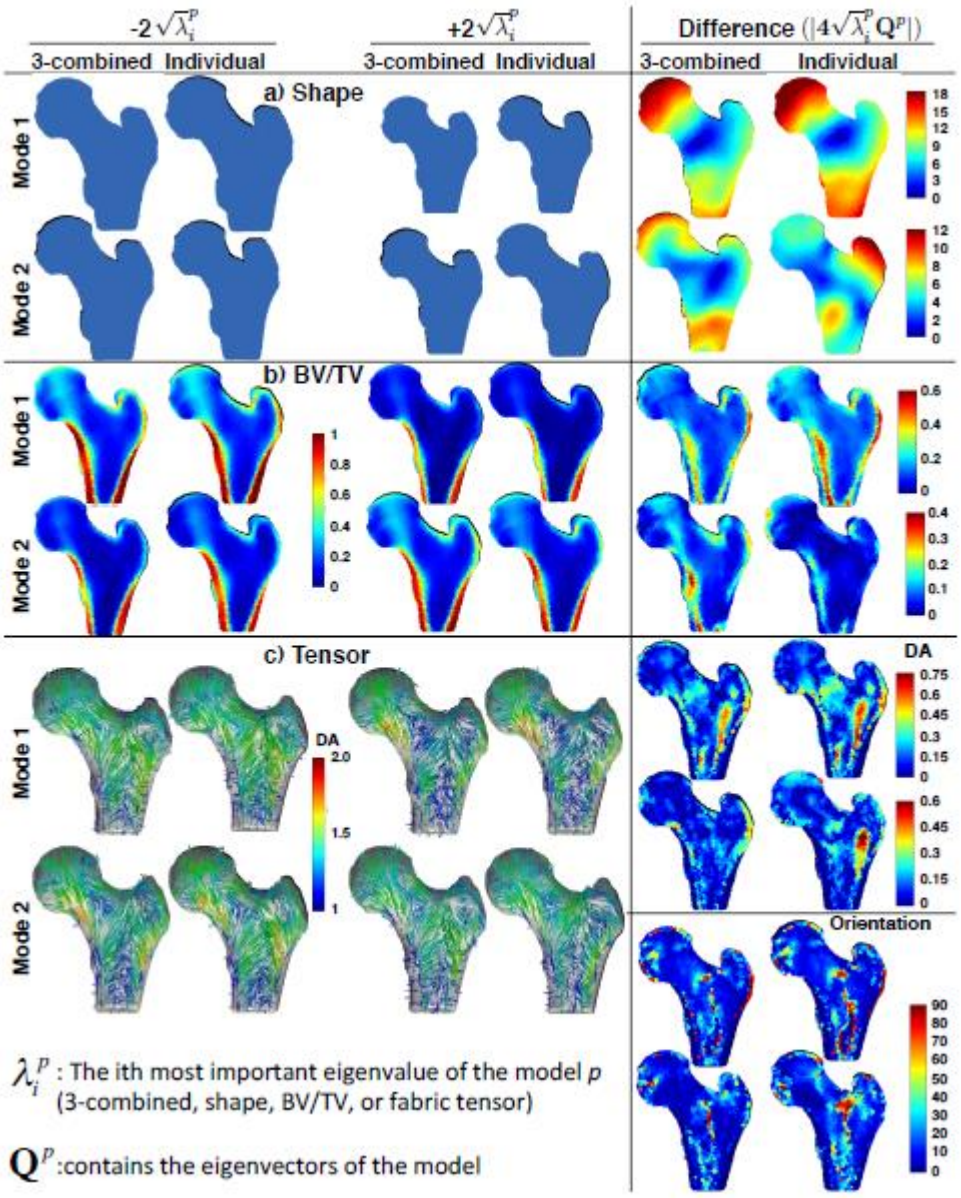

Figure 2. The variation represented for (a) shape, (b) BV/TV, (c) and the fabric tensor by the first two modes of individual models and the 3-combined model. For each model, the bone variations for -2 and +2 times the standard deviation ($\sqrt{\lambda_i^p}$) from the average in direction of the corresponding modes are represented. The values for BV/TV and the tensor are shown on the average bone. The two rightmost columns show the absolute difference between the reconstructed parameters by -2 and +2 times the standard deviation with respect to the average. The difference in the fabric tensor orientation is shown as the angle between principal orientations of reconstructed tensor at the two extremes of each mode for each element. The color-maps are adapted for the differences in each mode for visualization purposes (Refer to the animations in supplementary material for a better visualization of different modes of the statistical models).

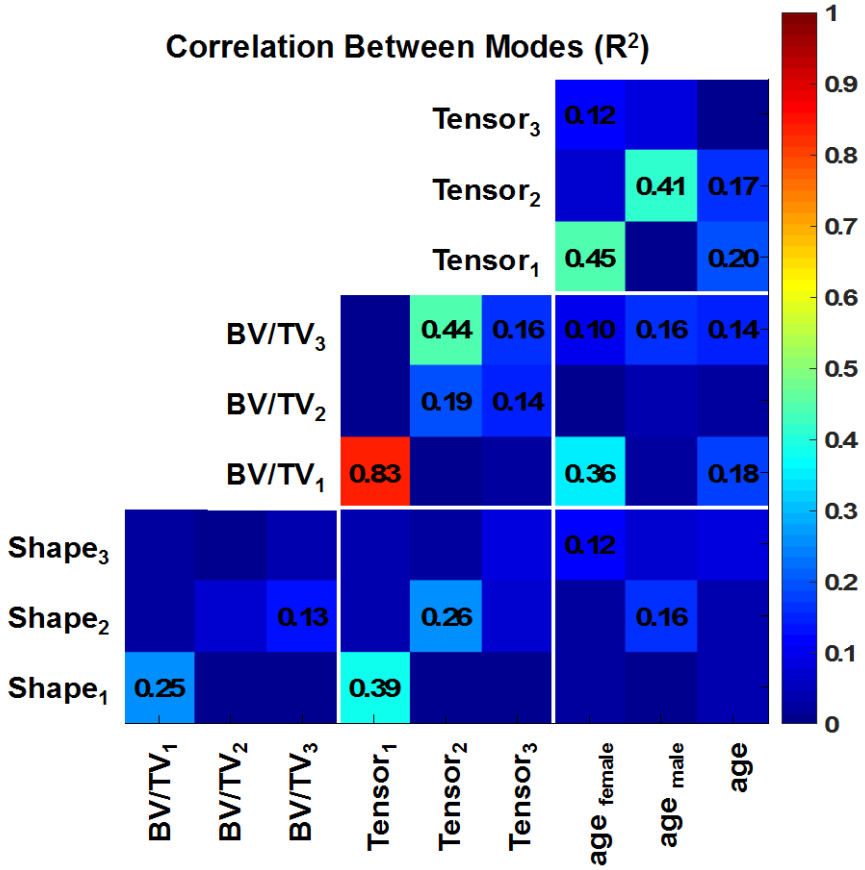

Figure 3. The correlation between the first three modes of shape, BV/TV, and tensor models are shown with respect to each other and with respect to age. The value given in each cell corresponds to the R^2 of the correlation. A single strong correlation (R^2 = 0.8) was found between the first mode of BV/TV and the first mode of tensor.

The ability of different models to reproduce femoral bones has been evaluated using the generalization error (Figure 4). As expected, increasing the number of modes decreased the generalization error for the model of shape and BV/TV. The generalization error decreases respectively by 60% and 40% for the model of shape and BV/TV, compared to their values predicted by the mean bone. However, the generalization error remained nearly constant for increasing number of modes for the fabric tensor; the relative improvement was less than 1% for orientation and 10% for the DA when using all modes of the statistical model. In addition, the combined model showed a very similar behavior as each of the individual models. Of course, the number of modes was adjusted to describe the equivalent variability, i.e. the initial model of the 3-combined model corresponds to three modes of the individual models, since this single mode encodes at the time, shape, BV/TV and bone fabric. Again, the generalization error remained constant for the bone fabric, which indicates that little information is contained in the fabric model beyond its average and the initial mode.

In addition, the similarity between the generalization error of the individual and combined models further confirms the independence of the individual models and therefore indicates that the combined model does not encode additional correlation between the parameters.

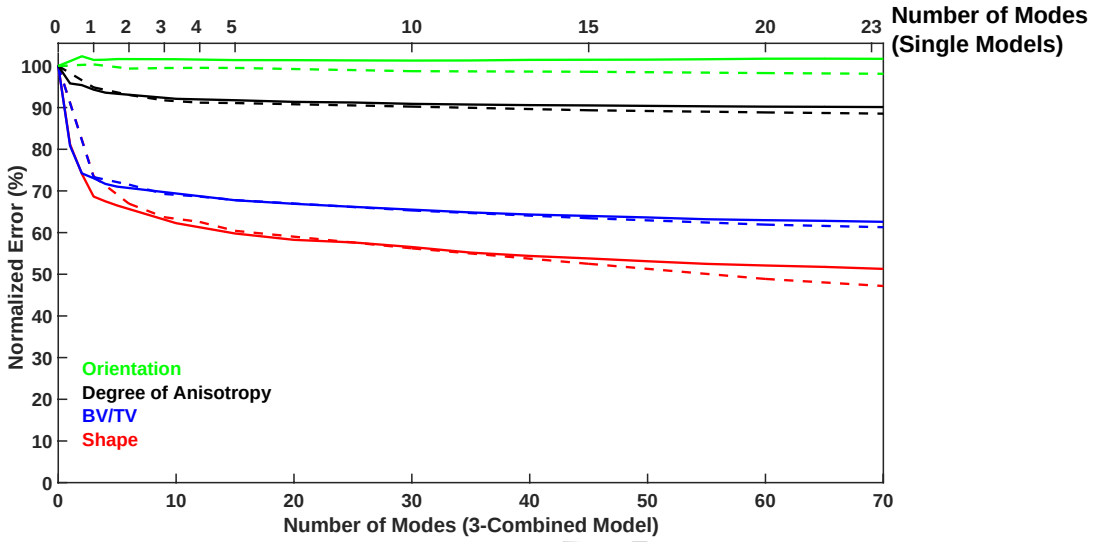

Figure 4. Normalized generalization error of each individual (dotted line) and 3-combined (solid line) models. The generalization ability of the model describing bone fabric is shown with two metrics; the error predicting the orientation and the error on the reconstructed DA (subsection 2.5.1). Two abscissa axes are shown in the figure, one on the bottom for 3-combined model, and one on the top for the individual models.

Finally, the compactness of the three individual models was calculated. The shape model was the most compact model followed by the BV/TV model (Figure 5). For these models, the first mode accounts for about 50% of the variability in the population, while 30 modes are sufficient to represent 90% of the existing bone shape or intensity. On the other hand, the compactness of the tensor model was low, starting with 7% of the total energy for the first mode of the model and not changing much for other modes. These results suggest that there is no information in the different tensor modes and therefore only the average model is sufficient to describe the bone fabric for all the samples in the dataset. Instead of using statistical model to predict fabric tensor, we propose to use average bone fabric in the FE simulations.

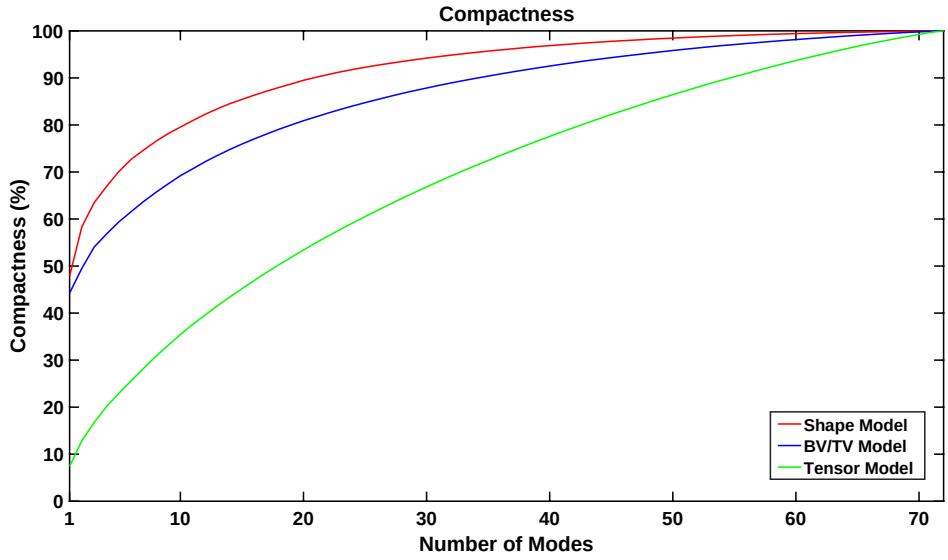

Figure 5. The compactness of each individual model. The tensor model showed a low compactness; the initial model represent only 10% of the variability and almost all the modes are required to reach 90% of the variability. Compactness calculated for the bone shape and BV/TV correspond to previous reports [17].

3.2 Mechanical Evaluation

The FE simulations were performed for three models with (1) anisotropic information extracted from HR-pQCT scans (the original model), (2) the average anisotropy and (3) isotropic material properties.

The numerical model was first validated against experimental data. Results showed that the FE calculation using the anisotropic information extracted from the HR-pQCT scan was able to accurately predict the experimental measurements. On the 10 samples used for the validation, the correlation between ultimate force calculated numerical and the experimental results was R^2=0.81 with a slope of 1.02. The displacement at the maximum force in the force-displacement curve (ultimate displacement) was also accurately predicted with a correlation of R^2=0.61 and a slope of 0.96. The results of the pairwise t-test indicated that there is no statistically significant difference between the experimental data and the simulation results. The comparison between isotropic material properties and the experiment shows that the isotropic material does not represent the biomechanical properties of the bone as accurately as the patient-specific anisotropy (Figure 6). While the correlation coefficient was similar to the patient-specific models, the slope of the isotropic calculations is about 0.85, which differs from the line of equality. Moreover, t-test showed a significant difference between the ultimate force and displacement

calculated using hFE model with isotropic material properties and the values measured in the experiments (pF = 0.01 and pU = 0.03).

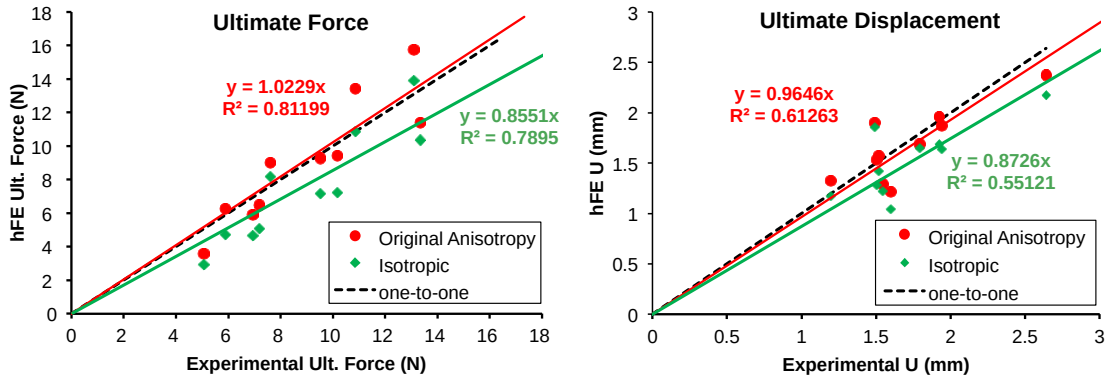

(a) (b)

Figure 6. The ultimate force and displacement, calculated for patient-specific hFE model (red circles) and hFE model based on isotropic material (green diamonds) vs. the results measured in the experimental setup.

The validated hFE model was used to evaluate the mechanical effect of different approach to assign bone fabric. The average fabric tensor (no mode of variation was included) was able to accurately estimate the ultimate force calculated by patient-specific hFE model (error of about 4%), while the isotropic model showed a prediction error about 4.5 times higher (about 18.4%). A similar observation was obtained for the prediction of the ultimate displacement where the average fabric resulted in a small prediction error (about 3%), which was about 3 times lower than the prediction error achieved with the isotopic model (about 9%). In addition, no statistically significant difference was observed between the results calculated with the original model and the model based on average anisotropy (p=0.557 and p=0.076 for respectively, ultimate force and ultimate displacement) while the comparison with the isotropic model showed statistically significant differences (p<0.001), compared to both the original model and the average anisotropy model. Finally, the ANCOVA test showed a statistically significant difference between average fabric tensor and isotropic material, for both ultimate force and ultimate displacement (p<0.001).

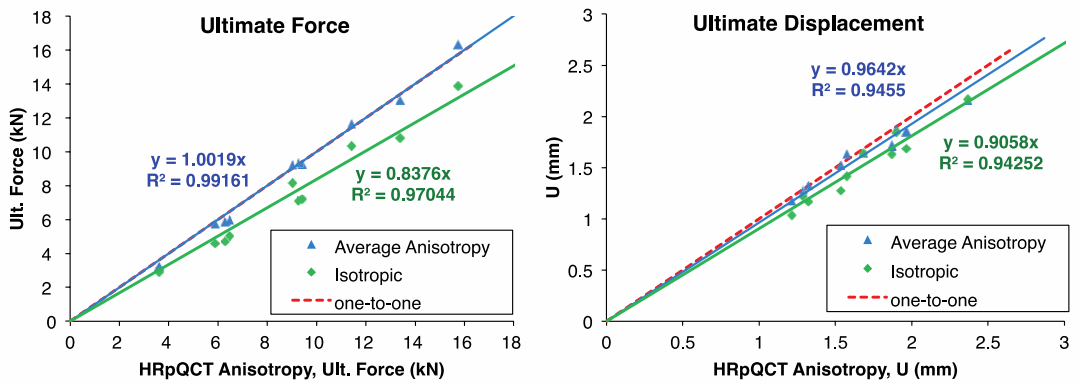

(a) (b)

Figure 7. The ultimate force and displacement, calculated for average anisotropy (blue triangles) and isotropic material (green diamonds) vs. the results calculated for original anisotropy based on HR-pQCT.

In general, the model with average anisotropy provides similar FE results as the model directly derived from the patients' HR-pQCT image. However isotropic material properties failed to predict the results of the patient-specific anisotropy. The results obtained with the average fabric tensor were similar to those obtained using the original anisotropy in the stance position while the isotropic material underestimates the ultimate force and displacement (Figure 7).

4 Discussion

Statistical models have been used to study the variation of bone properties, improve implant design and build patient-specific FE models [26–30]. However existing models focused on bone shape and to some extent to bone density, but overlooked the anisotropy of trabecular bone. Including fabric information in these statistical models would help to gain a deeper understanding of its variation in the population. In addition, this variation could be studied with respect to the shape of the bone as well as BV/TV using combined statistical models.

While many studies analyzed the correlation of bone micro-architectural parameters to bone strength and fracture risk [1,12,31–34], the relations between the distribution of these parameters in the proximal femur were not known. However, these studies relied on correlations based on local bone properties and were not modeling the change of the overall distribution of bone density and fabric between specimens. Our results showed that there is no correlation between the distributions of bone shape, BV/TV, and fabric. Therefore it is not possible to gain information on the DA from the shape or density of the patient's bone. A correlation was only found between the

first parameters of bone fabric and of the first mode of BV/TV, but all remaining correlations were insignificant. This finding is inline with previously published results showing that the DA was scarcely in correlation with BV/TV in the femoral head [35,36].

In addition, the statistical model of bone fabric indicated that trabecular bone orientation and DA did not vary significantly within the population. Therefore, the map of bone orientation in the proximal femur can be assumed to be constant among patients and that the average orientation is a good predictor of the patient's fabric. Of course, the average orientation did not perfectly represent the individual bone orientation; the average difference between the principal orientation and the corresponding ground-truth was 17°, with 10.4% error on prediction of the DA. However, this prediction error corresponds to previous studies [7–9,11,37]. Two alternative techniques were tested to improve the prediction of fabric orientation compared to the global alignment obtained by Procrustes; first bone fabric was aligned based on the local orientation of the elements. The second approach relied on the orientation of the bone fabric based on the orientation of larger regions of the femur such as the femoral head, neck, greater trochanter, and shaft). The local adaptation of the fabric orientation improved the predictions of principal fabric orientation by two degrees, however it did not have measurable influence on the mechanical behavior. Based on this observation, we decided to use average anisotropy without local orientation adaptation, since this approach proved to provide a similar level of accuracy as more complex techniques.

The stability of the bone orientation within the population was confirmed by mechanical simulation of the proximal femur using finite elements analyses; using the average bone fabric lead to mechanical results identical to the ground truth model directly built from HR-pQCT and significantly improve the mechanical simulations compared to a model relying on isotropic mechanical properties. The good prediction of the mechanical evaluation with the average anisotropy map is in agreement with previous results showing that morphing the fabric information of the template anisotropy is able to reproduce a mechanical behavior of the proximal femur. In this context, the average of the anisotropic calculated in the present work can be seen as the optimal approach to select the template anisotropy for the registration approach.

Only one existing study investigated the inter-individual variability of bone density and DA [15]; computational methods were used to study the inter-individual variability of BV/TV and DA in the entire proximal femur. A large variation was observed among the samples for the BV/TV while the inter-individual variability in DA was low. The outcomes of our statistical model also confirm that, not only the DA but also the distribution of fabric tensor in the proximal femur is near to constant and that large variation in the distribution of bone density were present in the statistical models of the population. Other studies focused on the age-dependence of the morphological parameters [14] and found a moderate correlation between age and DA for specific regions of the femoral head ($R^2 \approx 0.45$). A similar correlation was found in the present study between age and the initial modes of the tensor model describing bone fabric ($R^2 \approx 0.43$). However, it is important to note that the initial modes of the tensor model represent marginal information and that the correlation is therefore of limited value.

It is important to have enough samples in the models to represent the anatomical variations present in a population. In this study, 73 bones were included in the statistical models. These samples were either healthy, osteoporotic or osteopenic, but were mostly obtained from an elderly population. It is difficult to define the number of samples required to build relevant models and to determine what is the extent of the population represented by our samples. To estimate the effect of changing the size of the dataset, the statistical analysis was repeated using only half of the bone samples. Only small differences could be observed when using the reduced models; the average reconstruction error was slightly higher with only 36 samples compared to the complete model, but the overall differences remained small. Therefore, the number of sample included in the model seems to be a valid representation of the population. Nevertheless, the model built in this study only represents the training datasets and the validity of the results is therefore limited to elderly healthy, osteopenic, and osteoporotic patients.

Principal component analysis was used to represent the data and reduce the size of the model. The resulting modes of variations – described by the eigenvectors – are orthogonal, so it is possible to find the dependent and independent parameters among the bone. This property makes PCA a powerful tool in statistical modeling, but the "physical" interpretation of the different modes is difficult or even impossible beyond

the first few initial modes. However, most of the other matrix decomposition methods suffer from the same limitation and this approach was successful to establish correlation (or the absence of it) between the distributions of different bone parameters. Another limitation of PCA is that it finds only linear decomposition between parameters. Two sources of nonlinearities should be considered i) non-linear pattern in the distribution of anisotropy in the bone and ii) non-linear correlation between the distribution of anisotropy and bone shape or BV/TV. The first aspect has been considered and the analysis of the fabric tensors – which is positive semi-definite – has been analyzed using the log-Euclidean framework proposed by Arigny et al. [22]. The results of this analysis indicated that there is no significant variation in bone anisotropy, which implies that no nonlinearity arises from the relationship between fabric tensor with shape and/or BV/TV. For these reasons – and in order to limit the complexity of the analysis – linear PCA was used in this study.

The mechanical evaluations were performed with loading conditions corresponding to a stance position. With this loading environment, results showed that the average fabric orientation was able to reproduce the expected mechanical behavior. For a complete evaluation, additional loading conditions could be performed - typically, side fall. Nevertheless, Luisier et al. showed that the output of FE models with isotropic material properties is not significantly different from an FE model with anisotropic material properties [16]. Therefore, side-fall configuration is not expected to show the effect of anisotropy prediction on the bone stiffness. The cortical thickness was also not explicitly included in the FE model. Although, the mechanical simulations closely match the experimental data, a possible extension of the model is to build a statistical model describing the spatial distribution of the cortical thickness in the population. This information can be accurately derived from high-resolution scans and combined with the models of shape and/or bone intensity.

Based on these results, while it is not possible to accurately predict the fabric tensor distribution from the bone shape and the distribution of BV/TV, using the average fabric information makes it possible to predict the strength of the proximal femur. More studies on larger datasets - including pathological cases – as well as additional anatomical sites should be performed to confirm the conclusions of this study and show that it is possible to easily include fabric tensor information in the numerical simulation derived from clinical CT, provided that an average model of the anatomical site has been pre-established from high-resolution datasets.

Acknowledgement

The authors would like to thank Dr. Enrico Dall'Ara for sharing femoral data and Dr. Jakob Schwiedrzik and Dr. Dieter Pahr for providing the UMAT. Funding from the Swiss National Science Foundation (SNF) with grant no 143769 is gratefully acknowledged.

5 References

[1] G. Maquer, S.N. Musy, J. Wandel, T. Gross, P.K. Zysset, Bone volume fraction and fabric anisotropy are better determinants of trabecular bone stiffness than other morphological variables., J. Bone Miner. Res. 30 (2015) 1000–8. doi:10.1002/jbmr.2437.

[2] S.N. Musy, G. Maquer, J. Panyasantisuk, J. Wandel, P.K. Zysset, Not only stiffness, but also yield strength of the trabecular structure determined by non-linear μFE is best predicted by bone volume fraction and fabric tensor, J. Mech. Behav. Biomed. Mater. 65 (2017) 808–813. doi:10.1016/j.jmbbm.2016.10.004.

[3] C. Kober, B. Erdmann, C. Hellmich, R. Sader, H.-F. Zeilhofer, Consideration of anisotropic elasticity minimizes volumetric rather than shear deformation in human mandible., Comput. Methods Biomech. Biomed. Engin. 9 (2006) 91–101. doi:10.1080/10255840600661482.

[4] C. Hellmich, C. Kober, B. Erdmann, Micromechanics-based conversion of CT data into anisotropic elasticity tensors, applied to FE simulations of a mandible., Ann. Biomed. Eng. 36 (2008) 108–22. doi:10.1007/s10439-007-9393-8.

[5] N. Trabelsi, Z. Yosibash, Patient-specific finite-element analyses of the proximal femur with orthotropic material properties validated by experiments., J. Biomech. Eng. 133 (2011) 61001. doi:10.1115/1.4004180.

[6] T. San Antonio, M. Ciaccia, C. Müller-Karger, E. Casanova, Orientation of orthotropic material properties in a femur FE model: A method based on the principal stresses directions, Med. Eng. Phys. 34 (2012) 914–919. doi:10.1016/j.medengphy.2011.10.008.

[7] J. Hazrati Marangalou, K. Ito, B. van Rietbergen, A novel approach to estimate trabecular bone anisotropy from stress tensors., Biomech. Model. Mechanobiol. (2014). doi:10.1007/s10237-014-0584-6.

[8] K. Lekadir, J. Hazrati-Marangalou, C. Hoogendoorn, Z. Taylor, B. van Rietbergen, A.F. Frangi, Statistical estimation of femur micro-architecture

using optimal shape and density predictors., J. Biomech. 48 (2015) 598–603. doi:10.1016/j.jbiomech.2015.01.002.

[9] V. Chandran, P. Zysset, M. Reyes, Prediction of Trabecular Bone Anisotropy from Quantitative Computed Tomography using Supervised Learning and a Novel Morphometric Feature Descriptor, in: MICCAI, Munich, 2015.

[10] S.M. Nazemi, D.M.L. Cooper, J.D. Johnston, Quantifying trabecular bone material anisotropy and orientation using low resolution clinical CT images: A feasibility study, Med. Eng. Phys. 38 (2016) 978–987. doi:10.1016/j.medengphy.2016.06.011.

[11] E. Taghizadeh, M. Reyes, P. Zysset, A. Latypova, A. Terrier, P. Büchler, Biomechanical Role of Bone Anisotropy Estimated on Clinical CT Scans by Image Registration, Ann. Biomed. Eng. 44 (2016) 1–13. doi:10.1007/s10439-016-1551-4.

[12] T.E. Ciarelli, D.P. Fyhrie, M.B. Schaffler, S.A. Goldstein, Variations in three-dimensional cancellous bone architecture of the proximal femur in female hip fractures and in controls., J. Bone Miner. Res. 15 (2000) 32–40. doi:10.1359/jbmr.2000.15.1.32.

[13] J. Homminga, B.. McCreadie, T.. Ciarelli, H. Weinans, S.. Goldstein, R. Huiskes, Cancellous bone mechanical properties from normals and patients with hip fractures differ on the structure level, not on the bone hard tissue level, Bone. 30 (2002) 759–764. doi:10.1016/S8756-3282(02)00693-2.

[14] W.-Q. Cui, Y.-Y. Won, M.-H. Baek, D.-H. Lee, Y.-S. Chung, J.-H. Hur, et al., Age-and region-dependent changes in three-dimensional microstructural properties of proximal femoral trabeculae., Osteoporos. Int. 19 (2008) 1579–87. doi:10.1007/s00198-008-0601-7.

[15] J. Hazrati Marangalou, K. Ito, F. Taddei, B. van Rietbergen, Inter-individual variability of bone density and morphology distribution in the proximal femur and T12 vertebra., Bone. 60 (2014) 213–20. doi:10.1016/j.bone.2013.12.019.

[16] B. Luisier, E. Dall'Ara, D.H. Pahr, Orthotropic HR-pQCT-based FE models improve strength predictions for stance but not for side-way fall loading compared to isotropic QCT-based FE models of human femurs., J. Mech.

Behav. Biomed. Mater. 32 (2014) 287–99. doi:10.1016/j.jmbbm.2014.01.006.

[17] S. Bonaretti, C. Seiler, C. Boichon, M. Reyes, P. Büchler, Image-based vs. mesh-based statistical appearance models of the human femur: Implications for finite element simulations., Med. Eng. Phys. 36 (2014) 1626–35. doi:10.1016/j.medengphy.2014.09.006.

[18] S. Klein, M. Staring, K. Murphy, M. a Viergever, J.P.W. Pluim, Elastix: a Toolbox for Intensity-Based Medical Image Registration., IEEE Trans. Med. Imaging. 29 (2010) 196–205. doi:10.1109/TMI.2009.2035616.

[19] D.H. Pahr, P.K. Zysset, From high-resolution CT data to finite element models: development of an integrated modular framework, Comput. Methods Biomech. Biomed. Engin. 12 (2009) 45–57. doi:10.1080/10255840802144105.

[20] T.F. Cootes, C.J. Taylor, D.H. Cooper, J. Graham, Active Shape Models-Their Training and Application, Comput. Vis. Image Underst. 61 (1995) 38–59. doi:10.1006/cviu.1995.1004.

[21] R.O. Duda, P.E. (Peter E. Hart, D.G. Stork, Pattern classification, Wiley, 2001.

[22] V. Arsigny, P. Fillard, X. Pennec, N. Ayache, Log-Euclidean metrics for fast and simple calculus on diffusion tensors., Magn. Reson. Med. 56 (2006) 411–21. doi:10.1002/mrm.20965.

[23] P.T. Fletcher, S. Joshi, Riemannian geometry for the statistical analysis of diffusion tensor data, Signal Processing. 87 (2007) 250–262. doi:10.1016/j.sigpro.2005.12.018.

[24] D.H. Pahr, J. Schwiedrzik, E. Dall'Ara, P.K. Zysset, Clinical versus pre-clinical FE models for vertebral body strength predictions, J. Mech. Behav. Biomed. Mater. 33 (2014) 76–83. doi:10.1016/j.jmbbm.2012.11.018.

[25] E. Dall'Ara, B. Luisier, R. Schmidt, F. Kainberger, P. Zysset, D. Pahr, A nonlinear QCT-based finite element model validation study for the human femur tested in two configurations in vitro., Bone. 52 (2013) 27–38. doi:10.1016/j.bone.2012.09.006.

[26] T.L. Bredbenner, R.L. Mason, L.M. Havill, E.S. Orwoll, D.P. Nicolella, Fracture risk predictions based on statistical shape and density modeling of the proximal femur, J. Bone Miner. Res. 29 (2014) 2090–2100.

doi:10.1002/jbmr.2241.

[27] N. Sarkalkan, H. Weinans, A. a Zadpoor, Statistical shape and appearance models of bones., Bone. 60 (2014) 129–40. doi:10.1016/j.bone.2013.12.006.

[28] N. Sarkalkan, J.H. Waarsing, P.K. Bos, H. Weinans, A.A. Zadpoor, Statistical shape and appearance models for fast and automated estimation of proximal femur fracture load using 2D finite element models., J. Biomech. 47 (2014) 3107–14. doi:10.1016/j.jbiomech.2014.06.027.

[29] N. Kozic, S. Weber, P. Büchler, C. Lutz, N. Reimers, M.A. González Ballester, et al., Optimisation of orthopaedic implant design using statistical shape space analysis based on level sets., Med. Image Anal. 14 (2010) 265–75. doi:10.1016/j.media.2010.02.008.

[30] L. Grassi, E. Schileo, C. Boichon, M. Viceconti, F. Taddei, Comprehensive evaluation of PCA-based finite element modelling of the human femur., Med. Eng. Phys. 36 (2014) 1246–52. doi:10.1016/j.medengphy.2014.06.021.

[31] S. Boutroy, B. Van Rietbergen, E. Sornay-Rendu, F. Munoz, M.L. Bouxsein, P.D. Delmas, Finite element analysis based on in vivo HR-pQCT images of the distal radius is associated with wrist fracture in postmenopausal women., J. Bone Miner. Res. 23 (2008) 392–9. doi:10.1359/jbmr.071108.

[32] P. Pulkkinen, F. Eckstein, E.-M. Lochmüller, V. Kuhn, T. Jämsä, Association of Geometric Factors and Failure Load Level With the Distribution of Cervical vs. Trochanteric Hip Fractures, J. Bone Miner. Res. 21 (2006) 895–901. doi:10.1359/jbmr.060305.

[33] J.A. Cauley, P.M. Cawthon, K.E. Peters, S.R. Cummings, K.E. Ensrud, D.C. Bauer, et al., Risk Factors for Hip Fracture in Older Men: The Osteoporotic Fractures in Men Study (MrOS), J. Bone Miner. Res. 31 (2016) 1810–1819. doi:10.1002/jbmr.2836.

[34] E.M. Stein, A. Kepley, M. Walker, T.L. Nickolas, K. Nishiyama, B. Zhou, et al., Skeletal Structure in Postmenopausal Women With Osteopenia and Fractures Is Characterized by Abnormal Trabecular Plates and Cortical Thinning, J. Bone Miner. Res. 29 (2014) 1101–1109. doi:10.1002/jbmr.2144.

[35] T. Hildebrand, A. Laib, R. Müller, J. Dequeker, P. Rüegsegger, Direct Three-

Dimensional Morphometric Analysis of Human Cancellous Bone: Microstructural Data from Spine, Femur, Iliac Crest, and Calcaneus, J. Bone Miner. Res. 14 (1999) 1167–1174. doi:10.1359/jbmr.1999.14.7.1167.

[36] D. Ulrich, T. Hildebrand, B. Van Rietbergen, R. Müller, P. Rüegsegger, The quality of trabecular bone evaluated with micro-computed tomography, FEA and mechanical testing., Stud. Health Technol. Inform. 40 (1997) 97–112. http://www.ncbi.nlm.nih.gov/pubmed/10168885 (accessed December 5, 2016).

[37] J. Hazrati Marangalou, K. Ito, M. Cataldi, F. Taddei, B. van Rietbergen, A novel approach to estimate trabecular bone anisotropy using a database approach., J. Biomech. 46 (2013) 2356–62. doi:10.1016/j.jbiomech.2013.07.042.

6 Highlights

- A statistical model of the biomechanical properties of the proximal femur was built based on 73 HR-pQCT scans
- The correlation found among bone fabric, bone volume fraction, and bone shape was weak.
- The average fabric tensor is good predictor of patient-specific fabric tensor extracted from HR-pQCT scan.
- Finite element calculations based on the average bone orientation closely reproduces the bone strength obtained using patient-specific fabric tensor.
- Fabric of the proximal femur follows a similar structure within the population, which can be leveraged to build patient-specific models.